Constraining kinematic rotation axes in high-strain zones: a potential microstructural method?

STEVEN M. REDDY & CRAIG BUCHAN

Tectonics Special Research Centre, Department of Applied Geology, Curtin University of Technology, GPO Box U1987, Perth, WA 6845, Australia

(e-mail: S.Reddy@curtin.edu.au/C.Buchan@curtin.edu.au)

Abstract: The correct determination of the kinematic rotation axis in high-strain zones is essential to the study of the tectonic evolution of the Earth's crust. However, the common assumption that the kinematic rotation axis lies orthogonal to the XZ plane of the finite strain ellipse may be invalid in the case of general shear. Orientation data obtained by electron backscatter diffraction from calcite, deformed in the high-strain Gressoney Shear Zone of the Western Alps, has been investigated using orientation maps, bulk sample crystallographic orientation and misorientation analyses, and detailed intragrain misorientation and crystallographic dispersion analysis. The results demonstrate a strong geometrical coincidence amongst (1) the bulk macroscopic kinematic rotation axis, (2) the orientation of misorientation axes associated with low-angle boundaries, and (3) rotation axes associated with crystallographic dispersion at the intragrain scale. This coincidence is interpreted to reflect a geometric control of the kinematic framework of the high-strain zone on the activity of crystal slip systems. It is proposed that this relationship may be exploited as a new microstructural tool to determine the orientation of bulk kinematic rotation axes in high-strain zones without assuming a geometric link between kinematic rotation and XZ sections. Although further testing is required, application of the approach may lead to a significant advance in our understanding of natural general shear deformation.

Understanding the kinematic evolution of high-strain zones (HSZ) is essential for interpreting the tectonic evolution and palaeogeographic reconstruction of modern and ancient orogens. Commonly HSZ are assumed to have developed by simple shear, enabling mineral lineation orientations to be geometrically related to the transport direction (Ramsay 1980; Hanmer & Passchier 1991). However, theoretical modelling of 'general shear', involving simultaneous components of coaxial and non-coaxial shear, predicts patterns of deformation that are far more complex than those produced by end member pure and simple shear alone (Sanderson & Marchini 1984; Fossen & Tikoff 1993, 1998; Robin & Cruden 1994; Tikoff & Teyssier 1994; Jones *et al.* 1997; Tikoff & Greene 1997; Jiang & Williams 1998; Lin *et al.* 1998; Passchier 1998). One important complexity is that the kinematic rotation axis (or vorticity vector) of the deformation may not lie orthogonal to the orientation of maximum finite stretch indicated by mineral stretching lineations. Consequently, the XZ surfaces of HSZ may not be the correct surface from which to gather kinematic (shear sense) data.

Despite the importance of constraining tectonic transport direction, there are currently few criteria with which to quantify the orientation of the kinematic rotation axis that are independent of the assumption that mineral stretching lineations lie orthogonal to the kinematic rotation axis. This paper presents quantitative microstructural data obtained by electron backscatter diffraction (EBSD) of polycrystals deformed in an HSZ. The data demonstrate a geometric correlation between macroscopic kinematic rotation axes and both misorientation and dispersion axes associated with intragrain low-angle boundaries at the single and multiple grain scale. These observations indicate a potential means of constraining kinematic rotation axes that is independent of the orientation of mineral stretching lineations.

The data presented here come from a single calcschist sample (S3-74 located at N45°53′ E7°40′) taken from the Gressoney Shear Zone of the Western Italian Alps (Fig. 1), an HSZ documented in some detail in previous studies (Reddy *et al.* 1999, 2003; Wheeler *et al.* 2001*a*). The Gressoney Shear Zone is dominated by bulk top-to-SE extensional deformation that

From: GAPAIS, D., BRUN, J. P. & COBBOLD, P. R. (eds) 2005. *Deformation Mechanisms, Rheology and Tectonics: from Minerals to the Lithosphere*. Geological Society, London, Special Publications, **243**, 1–10.
0305-8719/05/$15.00

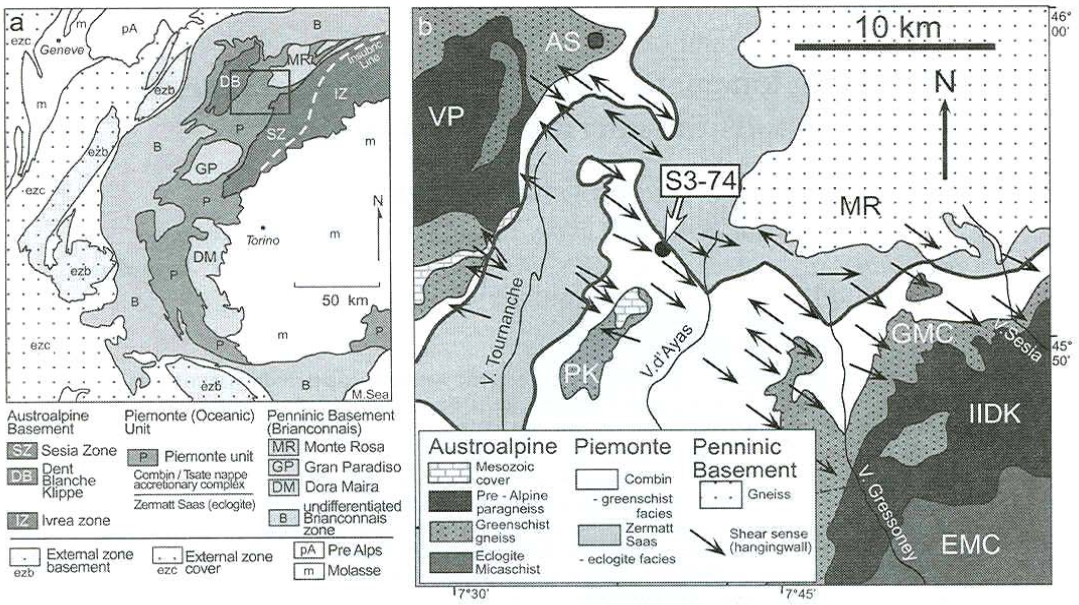

Fig. 1. Geological maps of the internal zones of the Alps (modified after Reddy *et al.* 2003). (**a**) Simplified geological map of the Western Alps; location of (b) marked by rectangular box. (**b**) Geological map of the internal zones of the Western Alps north of the Aosta Fault showing location of sample S3-74. Arrows indicate sense of shear with relative displacement of the hangingwall marked by the arrowhead. EMC, Eclogitic Micaschist Complex; GMC, Gneiss Minuti Complex; IIDK, Seconda Zona Diorito Kinzigitica; MR, Monte Rosa; AS, Arolla Schist; VP, Valpelline; PK, Pillonet Klippe. The heavy line indicates the contact between oceanic eclogite- and greenschist-facies rocks that mark the base of the Gressoney Shear Zone.

was responsible for exhumation of oceanic eclogite facies rocks from lower to mid-crustal levels between 45 and 36 Ma ago (Reddy *et al.* 1999, 2003). Conservative estimates of bulk strain indicate $\gamma > 50$ across the 1 km wide HSZ (Wheeler *et al.* 2001*a*). However this strain was spatially and temporally localized (Reddy *et al.* 2003) and in detail the Gressoney Shear Zone has a complex deformation history that may include kinematic partitioning (Reddy *et al.* 1999).

The analysed sample contains well-developed kinematic indicators, including shear bands and mica fish structures that could be observed in three dimensions in the field. At both the macro- and microscopic scales, mineral stretching lineations can be traced continuously into shear bands suggesting that the shear bands are a true reflection of the overall sense of shear (Reddy *et al.* 1999, 2003). The symmetry plane of these monoclinic fabric elements contains the mineral elongation, and the pole of this plane is interpreted to represent the kinematic rotation axis. This geometry indicates either deformation approximating simple shear or general shear deformation in which the coaxial stretching direction was subparallel to the non-coaxial maximum stretch component (Type E transpression of Fossen & Tikoff 1998). Since Gressoney Shear Zone deformation is not consistent with significant constrictional strain (Reddy *et al.* 1999, 2003) the former option is more likely. To summarize for sample S3-74, the kinematic rotation axis lies in the foliation plane, close to 90° from the mineral lineation and therefore subparallel to Y (Fig. 2), and the deformation is close to end-member simple shear.

Analytical procedure

An oriented petrographic thin section of the sample, cut parallel to the XZ section (XZ = 130.58NE, X = 16.321) was polished with progressively finer grades of diamond paste down to a 0.25 μm diamond polish. The section was then polished using a 0.06 μm colloidal silica suspension in a NaOH solution of pH 10 on a Buehler Vibromet II™ polisher. The sample was studied optically before being analysed in the scanning electron microscope (SEM). For EBSD analysis, the thin section was mounted in a Phillips XL30 SEM (operating conditions were 20 kV and spot size *c.* 0.7 μm) and tilted

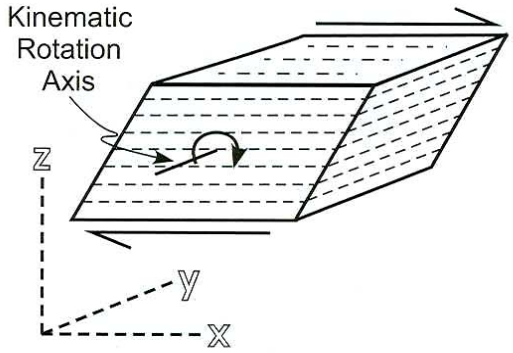

Fig. 2. Idealized HSZ coordinate reference frame used throughout this paper. The XY plane marks the shear plane of the HSZ with X the shear direction. In an HSZ deforming by simple shear the kinematic rotation axis corresponds to Y. Z marks the pole to the HSZ.

to 70°. Electron backscatter diffraction patterns (EBSPs) were obtained using an HKL Technology Nordlys detector and data were collected and processed using HKL Technology's Channel 5 software. Each EBSP was automatically matched by the Channel 5 software to theoretical EBSPs for calcite to give orientation information for each grid node. The closeness of fit between observed and theoretical patterns was good (average mean angular deviation = 0.62). Data were noise reduced using the Channel 5 'wildspike' correction and a four-neighbour zero solution extrapolation.

For this study a single orientation map was constructed by automatically collecting EBSPs from a user-defined grid of 120 × 70 points at 4 μm spacing (map area = 480 × 280 μm). The average grain diameter of the mapped area was 17 μm (range = 5–108 μm) with mean grain area of 347 μm^2. Zero solutions making up 18% of the map mostly reflect minor quartz and white mica in the sample. Channel 5 software was used to produce orientation maps, and calculate the minimum misorientation angle and misorientation axis geometry. The crystal symmetry of calcite means that a number of possible misorientation angles and axes may be calculated between two differently oriented crystals or parts of crystals. However, following several other workers, the angle/axis pair corresponding to the minimum misorientation angle was used for misorientation analysis (Pospiech *et al.* 1986; Mainprice *et al.* 1993; Lloyd *et al.* 1997; Wheeler *et al.* 2001*b*). This is justified for intragrain low-angle misorientation analysis.

Results

The results from a single orientation map (Fig. 3a) indicate a strong crystallographic preferred orientation (CPO) for most of the calcite grains analysed (cf. Fig. 3a, d). The orientation of the c-axis cluster is consistent with macroscopic kinematic indicators that record top-to-SE shearing (Fig. 3d). The only volumetrically significant exception to the CPO is grain 1 which has an a-pole parallel to the dominant c-direction in the sample (Fig. 3d). The uncorrelated misorientation angle distribution (Fig. 4a) indicates a smaller number of high misorientation angles than that predicted for a random distribution and is consistent with the presence of a CPO. The absence of a misorientation angle peak in the correlated data at 78° indicates that few of the calcite grains are twinned (e.g. Bestmann & Prior 2003). However, twinning is present in other parts of the sample.

The correlated misorientation angle distribution form the whole mapped area indicates numerous (*c.* 2000) low-angle boundaries between 2° and 10° (Figs 3a and 4a). These have orientations that cluster around the mesoscopic kinematic rotation axis (Y direction) of the sample (Fig. 4b). Although there are significant errors (up to 30°) associated with the determination of misorientations axes for small numbers of low-angle misorientations, these can be minimized by using a large dataset (Prior 1999). The clustering of *c.* 2000 low-angle misorientation axes around the centre of the pole figure (Fig. 4b) is statistically significant and is likely to reflect a geological process. Misorientation axes associated with correlated misorientation angles >10° have a random distribution (not shown), indicating no systematic relationship between the orientations of different calcite grains.

The qualitative distribution of low-angle boundaries (Fig. 3a) is shown in more detail for two grains (1 & 2) in which the orientation data has been coloured to demonstrate crystallographic orientation variations of 15° and 12° respectively from the (blue) centre of each grain (Fig. 3b, c). These data indicate that the variations in orientation across these grains are systematic, forming discrete bands of constant relative misorientation towards the grain edges (Fig. 3b, c). The overall bending of the crystal lattice is cumulative and there are no individual angular misorientations greater than 10° within either of the two grains. The systematic reorientation of crystal axes by low-angle boundaries is also apparent in pole figures of crystallographic orientation for grains 1 and 2 (Fig. 5) in which colour variations in the pole figures correspond

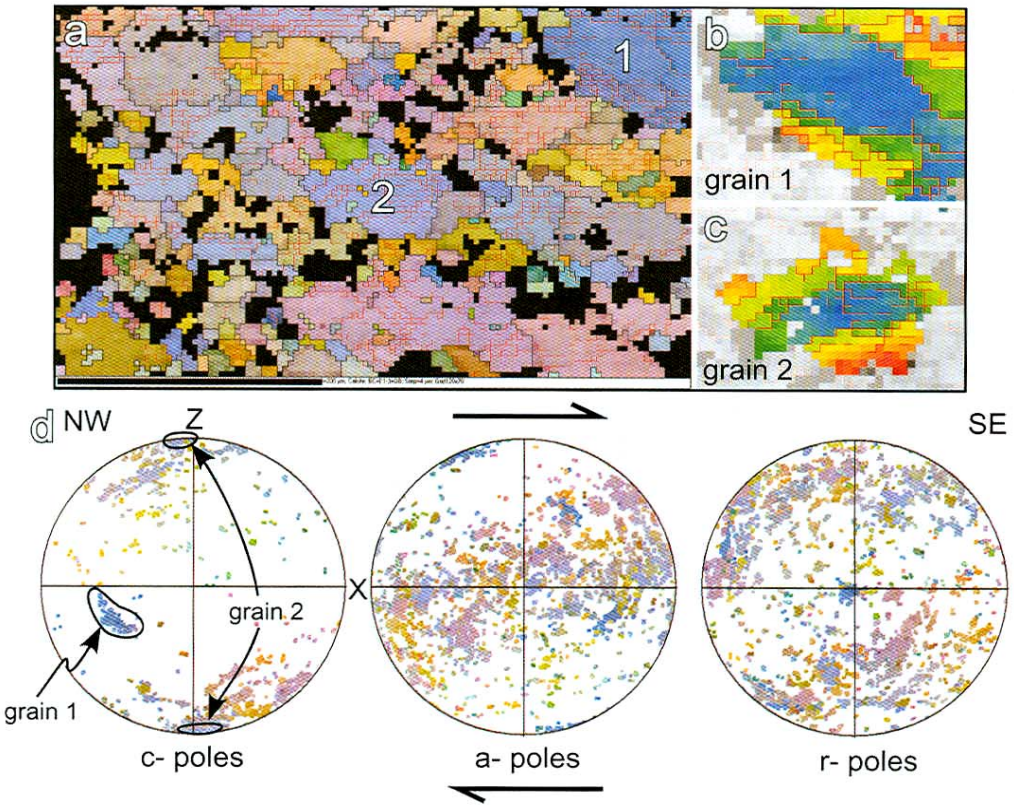

Fig. 3. (**a**) Automated EBSD map of calcite in S3-74 XZ (130.58NE) section. Each pixel (total = 6847) represents an individual orientation analysis. Colours reflect variations in orientation defined by the three Euler angles. Red and black lines represent boundaries with >2 and >10° misorientation respectively between adjacent analyses. Black pixels show analyses of quartz or white mica (data not shown) or zero solutions. Grains 1 and 2 correspond to grains shown in (b) and (c) respectively. (**b**) & (**c**) Detail of grains 1 (475 points) and 2 (304 points) derived by assigning a spectrum of colour (blue to red) to a range of 15° and 12° misorientations respectively from the centre of each grain. Systematic changes in colour indicate orientation variations due to low-angle boundaries. The spatial distribution of colours can be directly compared to crystallographic orientations indicated in Fig. 5. (**d**) Lower hemisphere, equal angle projections of calcite orientation data (c-, a- and r-poles) illustrated in (a). X and Z correspond to shear zone coordinates shown in Fig. 2. Colours in (a) correspond directly to position of orientation data in (d). Orientation data from grains 1 and 2 are indicated.

to the colours in the respective orientation maps (Fig. 3b, c).

The crystallographic axes within two grains of different bulk crystallographic orientation (grains 1 & 2) are dominantly dispersed around small circles centred on the centre of the pole figures, that is, the macroscopic Y direction of the shear zone coordinate system (Fig. 5a, b). In both grains, one crystallographic axis at the centre of the pole figures shows little dispersion (grain 1 = r-pole; grain 2 = a-pole). The relative lack of dispersion of this crystallographic orientation indicates that this represents a principal rotation axis associated with low-angle boundary formation within the grains.

In detail there are subtle complexities to this simple picture. In grain 1 there is slight dispersion of the central r-pole and other crystallographic axes that indicate minor dispersions away from a single small circle distribution centred around Y. The exact orientation of this second rotation axis is difficult to constrain due to the limited total angular dispersions associated with this axis (<5°). However it is interpreted to lie in the lower left quadrant of the pole figure. In grain 2, a second minor dispersion seemingly

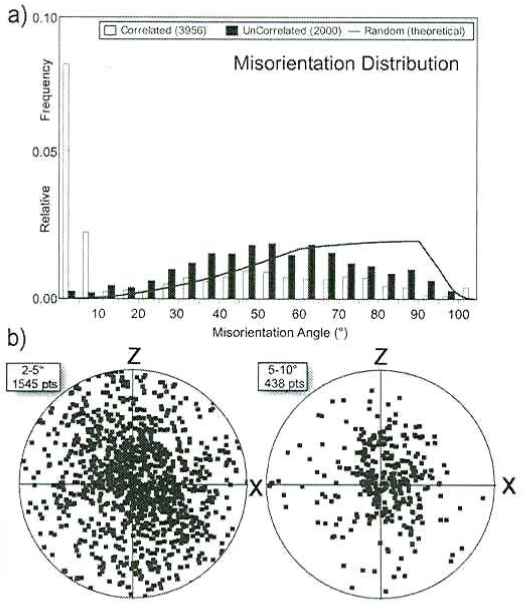

Fig. 4. (**a**) Minimum misorientation angle distribution for orientation data indicated in Fig. 3a. White histogram corresponds to neighbour-pair misorientations (correlated data), the black histogram representing random-pair misorientations (uncorrelated data). Uncorrelated data show a subsample of 2000 randomly chosen random-pair misorientations. Solid black line indicates the theoretical misorientation angle distribution of randomly oriented trigonal minerals. (**b**) The distribution of misorientation axes for minimum correlated misorientation angles of 2–5° and 5–10° shown in (a). These data indicate a concentration of low-angle misorientations axes around the sample Y direction.

around small circles centred around the f-pole in the lower right quadrant accommodates a few degrees of rotation. In both cases these additional rotational components are minor and only slightly modify the dominant dispersion centred around the sample Y direction, that is, the r-pole and a-pole for grain 1 and 2 respectively.

Misorientation axes for 2–5° and 5–10° minimum correlated misorientation angles plotted with respect to sample coordinates for grains 1 & 2 show a relatively widespread distribution (Fig. 6a, b, e, f). This is particularly evident for the 2–5° misorientation data. Such a result is expected because of large errors involved with calculating misorientation axes associated with low-angle misorientations (Prior 1999). However, in general the average distribution of misorientation axes is again close to the Y direction of the shear zone coordinate system (Fig. 2). The inverse pole figures showing the position of misorientations axes with respect to the crystal coordinate system (Fig. 6c, d, g, h) indicate very little preferred orientation.

Discussion

Calcite deformation and the role of different slip systems

In two grains of differing orientation, the dispersion of crystallographic axes associated with low-angle boundaries appears to be dominated by rotation about an axis that lies parallel to the kinematic Y direction of the sample (Fig. 5). For grain 1, the rotation axis associated with the dispersion of crystallographic axes has an orientation that corresponds to an r-pole (Fig. 5). The dominance of a single dispersion axis for this grain suggests that most deformation was accommodated on low-angle boundaries developed by activity of a single crystallographic slip system. However, the obliquity of low-angle boundary traces on the orientation map (Fig. 3b), and the presence of a second minor dispersion axis (Fig. 5a), indicates the presence of at least one other slip system. Similarly, low-angle boundaries in grain 2 (Fig. 5) also developed by multiple slip systems but were dominated by dispersion around an axis parallel to one of the a-poles.

The correlation of axes associated with dominant crystallographic pole dispersion with different crystallographic directions in grains 1 and 2 (r-pole and a-pole respectively) indicates that the dominant slip systems were different in the two grains. Crystallographic pole dispersion patterns can be used to identify intragrain slip systems using simple models of tilt boundary formation during the formation of edge dislocations (Lloyd & Freeman 1991, 1994). For tilt boundaries, the rotation axis for crystal slip is the normal to the plane that contains the pole to the slip plane and the slip direction, and therefore the three features are mutually orthogonal in calcite (De Bresser 1991; Bestmann & Prior 2003). Given that the dispersion axis lies in the centre of the pole figure, the slip plane and slip direction responsible for dispersion must lie on the primitive circle of the pole figure. Using this model, the data from grain 1 indicate the probability of a-slip ((-12-10) ⟨-2021⟩) as the active slip system. Experimental evidence for a-slip in calcite is rare (Turner & Heard 1965; Paterson & Turner 1970) and consequently is largely ignored as an important slip system (e.g. De Bresser & Spiers 1997). However, no other published calcite slip systems readily account for the observed dispersion around the r-pole (Fig. 5a). In addition, Schmid Factor

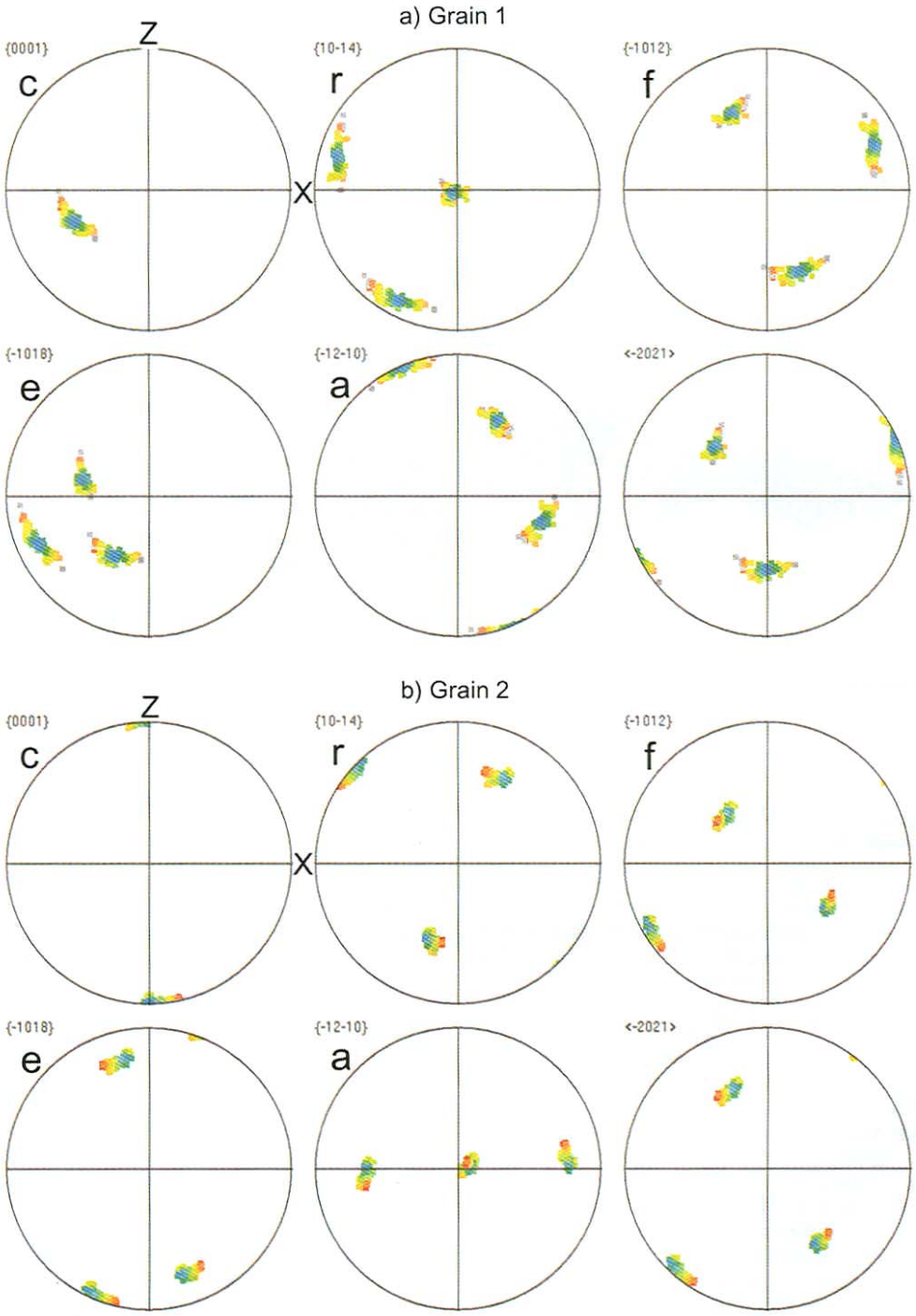

Fig. 5. Equal area, lower hemisphere projections of orientation data (poles to c, r, f, e, a and direction ⟨-2021⟩) for grains 1 and 2 of Fig. 3. In both grains most orientation data are dispersed in small circles around the centre of the pole figures. Dispersion axes are coincident with the r- and a-pole in grain 1 and 2, respectively. Minor secondary dispersion in both grains can also be identified and relates to the operation of secondary minor slip systems that cumulatively accommodate a few degrees of rotation.

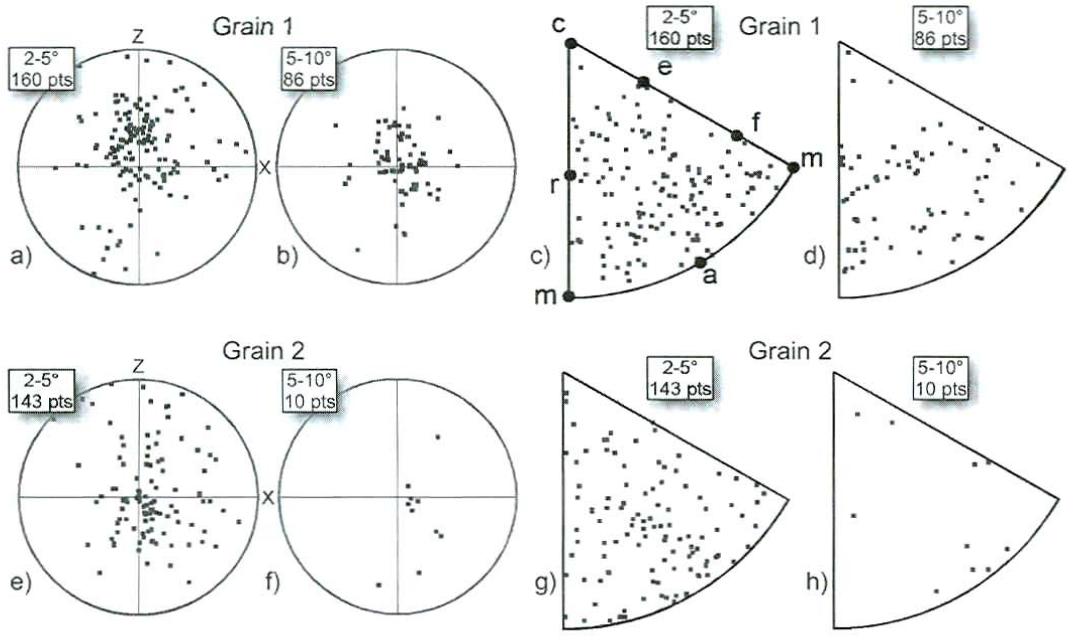

Fig. 6. Equal area, lower hemisphere projections of minimum misorientation axes orientation for low-angle boundaries in grains 1 and 2 plotted in both sample coordinate (pole figure) and crystal coordinate (inverse pole figure) space for misorientation angles of 2–5° and 5–10°.

analysis, assuming deformation was by simple shear, indicates higher resolved shear stress associated with a-slip (Schmid Factor = 0.5) than any other calcite slip system, further supporting the possibility of a-slip in grain 1. Since grain 1 is anomalous in its orientation (Fig. 3a, d) and makes up less than 5% of the analysed grains, its contribution to deformation of the sample as a whole is minor. The additional secondary dispersion axis identified in the pole figures (Fig. 5a) cannot be readily identified because of its small angular misorientations.

Grain 2 has an orientation similar to the majority of analysed grains and records dispersion about the central a-pole. This dispersion axis is common to both of the common calcite slip systems r- and f-slip. However, only in the case of r-slip is the slip direction also lying on the primitive circle at 90° to the pole to the slip plane (*cf.* Bestmann & Prior 2003). This geometry discriminates between the two slip systems and indicates the probability that the major dispersion in grain 2 was accommodated by r-slip ((10-14) ⟨-2021⟩). Importantly, despite the different slip systems, the rotation axis associated with low-angle boundary formation in both grains lies parallel to the macroscopic kinematic rotation axis (Y), suggesting a kinematic control on the activity of the dominant slip systems.

The recognition of specific crystallographic dispersion axes for grains 1 and 2 should also be recorded by the geometry of low-angle misorientation axes both in sample and crystal coordinate systems (Fig. 6). However, the misorientation data are not easily reconciled with the crystallographic pole dispersion data. Despite having an average orientation close to the Y axis, misorientation axes plotted in the sample coordinate system have a distribution that demonstrates a large degree of variation, particularly in the lower (2–5°) misorientations angles (Fig. 6a, b, e, f). The apparent almost random distribution of misorientation axes in the crystal coordinate system (Fig. 6c, d, g, h) is also inconsistent with the specific crystallographic dispersion axes identified earlier (Fig. 5), which would be expected to cluster around r- and a-poles for grains 1 and 2 respectively. There are several possible reasons for the observed discrepancy between the crystal pole dispersion axes and the misorientation axes.

Misorientation axes calculated from small angular misorientations have a significant error (tens of degrees) associated with them (Prior 1999). Such an error is significant in sample coordinate space (Prior 1999) and is amplified in crystal coordinate space where axes are plotted in a smaller angular volume. The error

associated with the calculation of misorientation axes decreases with increasing misorientation angle (Prior 1999) and it is noticeable that in grain 1, where we have sufficient 2–5° and 5–10° misorientations to make a comparison, that the distribution of, the misorientation axes for the larger misorientation angles is more tightly clustered around the kinematic Y direction (Fig. 6b). Furthermore, the 5–10° misorientation axes in crystal coordinate inverse pole figures (Fig. 6d) are less variable than the 2–5° axes (Fig. 6c). At least part of the variation in the distribution of misorientation axes is therefore attributed to errors associated with the calculation of misorientation axes for small angular variations.

The misorientation axis is the common axis between two different crystallographic orientations around which a rotation through the misorientation angle will bring the two orientations into coincidence (Pospiech *et al.* 1986). As such it is a geometric construct that need not relate to a specific process. Changes in orientation associated with a number of different slip systems may therefore yield misorientation axes that are a combination of the different slip systems and may not have simple relationships to crystallographic orientations (Lloyd & Freeman 1991). Although in both grains 1 and 2 the dominant slip system is associated with a crystallographic pole dispersion axis centred on the sample Y direction, the presence of other operating slip systems is also apparent from secondary dispersions. In grains 1 and 2, the secondary slip systems are minor and accommodate small misorientations so a combination of different slip systems should be more apparent in the 2–5° misorientations than in the larger misorientation angle data. Consequently, some of the variation in the orientation of 2–5° misorientation axes may be a result of a combination of minor amounts of slip on different slip systems.

As a result of the potential complications and the errors outlined above, individual misorientation axes are considered unreliable for identifying crystal slip systems associated with the development of low-angle boundaries. Dispersion axes obtained from crystallographic pole dispersion patterns (Fig. 5), particularly those illustrating a large cumulative angle of rotation, are considered to be a more robust method. However, the data presented here indicate that a large number of low-angle misorientation axes yield an average orientation that is identical to the rotation axis associated with crystallographic dispersion.

Many studies investigating slip systems within deforming minerals have recognized the importance of critically resolved shear stress (CRSS) for the initiation of slip on a particular slip system (e.g. Lister 1978; Takeshita *et al.* 1987 for calcite). The CRSS model assumes that slip on a particular system will occur when the shear stress on that slip system reaches a threshold value. Numerical investigations of slip systems in stress space indicate that the relative activity of these systems is controlled by the geometrical relationship of the yield surface to the imposed strain vector rather than the value of the CRSS (Lister & Hobbs 1980; Takeshita *et al.* 1987) suggesting that there is a geometrical control, in addition to a CRSS control, on slip system activity. The dispersion pattern dominated by a single rotation axis shown by our data suggests that activity is dominated by a single slip system in each grain, with a minor component of at least one other slip system. This is inconsistent with deformation as assumed in the Taylor models that consider single crystal yield surfaces requiring up to five active slip systems (Von Mises criteria) (Takeshita *et al.* 1987).

Taylor modelling ignores the effect of dynamic recrystallization and recovery that takes place in natural deformations, as well as other deformation processes such as diffusive mass transfer, diffusion accommodated grain boundary sliding and grain boundary migration that may relax the necessity for five active slip systems. Experimental studies involving dynamic recrystallization at high temperatures indicate that geometric softening associated with the preferred orientation of specific calcite slip systems may take place and lead to the accommodation of large shear strains (Pieri *et al.* 2001). Studies of dynamic recrystallization during natural deformation also indicate that within individual grains, deformation may be accommodated by the operation of a single slip system (Bestmann & Prior 2003). The data presented here are consistent with these findings and indicate a similar geometric control on the activity of particular slip systems, whereby the dominant slip system that operates within a particular deforming grain is one in which the geometric rotation axis associated with the slip system lies parallel to the mesoscopic kinematic rotation axis.

Microstructural characterization of the kinematic rotation axis

The data presented in this study demonstrate a geometrical coincidence of intragrain rotation axes responsible for the dispersion of crystallographic axes (Fig. 5), mean low-angle misorientation axes orientations from single crystals (Fig. 6),

low-angle misorientation axes collected from polycrystals (Fig. 4), and the macroscopic kinematic rotation axis of the HSZ. These observations indicate that rotation and misorientation axes associated with low-angle boundaries may provide geometric constraints on the orientation of the macroscopic kinematic rotation axis. This similarity of misorientation and rotation axes for low-angle boundaries with mesoscopic kinematic rotation axes has been noted previously in EBSD studies (e.g. Bestmann & Prior 2003), although the kinematic significance of this relationship has not been explored.

In this study, microscopic analysis has been linked to well-constrained kinematic data in which the shear direction of the studied HSZ has been previously established (Reddy *et al.* 1999, 2003). In this high-strain example the mineral lineation direction lies orthogonal to the kinematic rotation axis (Fig. 2). However, it cannot be assumed *a priori* that mineral stretching lineations lie orthogonally to the kinematic rotation axis. For example, in the case of general shear, the maximum finite stretch may be dominated by the coaxial component of the deformation that is independent of kinematic rotation. Despite this, mineral lineations are widely used to constrain shear directions and identify the ideal plane on which kinematic indicators should be viewed (XZ of Fig. 2). This may lead to incorrect interpretations of shear sense in HSZ deforming by general shear.

The data presented here indicate that for simple shear deformation the orientation of the kinematic rotation axis may be constrained by identifying the rotation axes associated with crystallographic dispersion across low-angle boundaries and geometrically coincident low-angle misorientation axes. Since crystallographic orientations are independent of the orientation of the analysed section, crystallographic dispersion and misorientation axes are readily identifiable from EBSD data independent of lineation orientation. Although the data presented here refer to conditions approaching simple shear, similar geometrical relationships may exist under general shear conditions. If so, the analysis of misorientation and dispersion axes may yield important information regarding the orientation of kinematic rotation axes in HSZ undergoing general shear. Further detailed studies are required to test this hypothesis.

Microstructural preservation and the temporal evolution of HSZ

Owing to the evolving nature of microstructures and their syn- and post-kinematic stability, low-angle boundaries may reflect only the last stages of the deformation history in a particular part of an HSZ. Consequently, kinematic information obtained from the analysis of low-angle boundaries may not represent much of the earlier kinematic evolution of the HSZ and may provide only a snapshot of the lattermost stages of deformation. This presents a problem in constraining variations of kinematic history during the temporal evolution of the HSZ. Recent detailed geochronological studies of the Gressoney Shear Zone indicate that the spatial distribution of deformation with time was heterogeneous, with strain migration and localization leading to the preservation of older parts of the shear zone between zones of younger deformation (Reddy *et al.* 1999, 2003). Preliminary microstructural data from other Gressoney Shear Zone samples, which record different deformation ages and variable kinematic senses, indicate that the Gressoney Shear Zone was not affected by a homogenous or pervasive, late-stage microstructural overprint and that microstructures (including low-angle boundaries) developed early in the deformation history may be preserved in different temporal domains. Therefore, different parts of the HSZ appear to have a microstructural memory that can be used to constrain the earlier parts of the deformation history. Consequently, the application of the technique presented in this paper to HSZ that record a complex evolution may lead to a significant advance in our understanding of kinematic partitioning in naturally deformed strain systems with respect to both space and time.

This work was funded through ARC Large Grant A00106036. The data presented in this paper were collected at the Australian Research Council (ARC) funded Microstructural Analysis Facility (part of the Western Australian Centre of Microscopy) at Curtin University of Technology, Perth, Australia. Geoff Lloyd, Neil Mancktelow and Denis Gapais are thanked for comprehensive and constructive reviews. This paper is TSRC publication No. 288 and contributes to the TSRC's Program 4: Tectonic Processes.

References

BESTMANN, M. & PRIOR, D. J. 2003. Intragranular dynamic recrystallisation in naturally deformed calcite marble: diffusion accommodated grain boundary sliding as a result of subgrain rotation recrystallization. *Journal of Structural Geology*, **25**, 1597–1613.

DE BRESSER, J. H. P. 1991. Intracrystalline deformation of calcite. *Geologica Ultrajectina*, **79**, 1–191.

DE BRESSER, J. H. P. & SPIERS, C. J. 1997. Strength characteristics of the r, f, and c slip systems in calcite. *Tectonophysics*, **272**, 1–23.

FOSSEN, H. & TIKOFF, B. 1993. The deformation matrix for simultaneous simple shearing, pure shearing and volume change, and its application to transpression – transtension tectonics. *Journal of Structural Geology*, **15**, 413–422.

FOSSEN, H. & TIKOFF, B. 1998. Extended models of transpression and transtension, and application to tectonic settings. *In*: HOLDSWORTH, R. E., STRACHAN, R. A. & DEWEY, J. F. (eds) *Continental Transpressional and Transtensional Tectonics.* Geological Society, London, Special Publications, **135**, 15–33.

HANMER, S. & PASSCHIER, C. W. 1991. Shear-sense indicators: a review. Geological Survey of Canada, Paper 90-17, 72.

JIANG, D. & WILLIAMS, P. F. 1998. High-strain zones: a unified model. *Journal of Structural Geology*, **20**, 1105–1120.

JONES, R. R., HOLDSWORTH, R. E. & BAILEY, W. 1997. Lateral extrusion in transpression zones: the importance of boundary conditions. *Journal of Structural Geology*, **19**, 1201–1217.

LIN, S., JIANG, D. & WILLIAMS, P. F. 1998. Transpression (or transtension) zones of triclinic symmetry: natural example and theoretical modelling. *In*: HOLDSWORTH, R. E., STRACHAN, R. A. & DEWEY, J. F. (eds) *Continental Transpressional and Transtensional Tectonics.* Geological Society, London, Special Publications, **135**, 41–57.

LISTER, G. S. 1978. Texture transitions in plastically deformed calcite rocks. *Proceedings of the 5th International Conference on Textures of Materials*, 199–210.

LISTER, G. S. & HOBBS, B. E. 1980. The simulation of fabric development during plastic deformation and its application to quartzite: the influence of deformation history. *Journal of Structural Geology*, **2**, 355–370.

LLOYD, G. E. & FREEMAN, B. 1991. SEM electron channelling analysis of dynamic recrystallization in a quartz grain. *Journal of Structural Geology*, **13**, 945–953.

LLOYD, G. E. & FREEMAN, B. 1994. Dynamic recrystallization of quartz under greenschist facies conditions. *Journal of Structural Geology*, **16**, 867–881.

LLOYD, G. E., FARMER, A. B. & MAINPRICE, D. 1997. Misorientation analysis and the formation and orientation of subgrain and grain boundaries. *Tectonophysics*, **279**, 55–78.

MAINPRICE, D., LLOYD, G. E. & CASEY, M. 1993. Individual orientation measurements in quartz polycrystals – advantages and limitations for texture and petrophysical property determinations. *Journal of Structural Geology*, **15**, 1169–1187.

PASSCHIER, C. W. 1998. Monoclinic model shear zones. *Journal of Structural Geology*, **20**, 1121–1137.

PATERSON, M. S. & TURNER, F. J. 1970. Experimental deformation of strained calcite crystals in extension. *In*: PAULITSCH, P. (ed) *Experimental and Natural Rock Deformation.* Springer, Berlin, 109–141.

PIERI, M., KUNZE, K., BURLINI, L., STRETTON, I., OLGAARD, D. L., BURG, J.-P. & WENK, H.-R. 2001. Texture development of calcite by deformation and dynamic recrystallization at 1000 K during torsion experiments of marble to large strains. *Tectonophysics*, **330**, 119–140.

POSPIECH, J., SZTWIERTNIA, K. & HAESSNER, F. 1986. The misorientation distribution function. *Textures and Microstructures*, **6**, 201.

PRIOR, D. J. 1999. Problems in determining the misorientation axes, for small angular misorientations, using electron backscatter diffraction in the SEM. *Journal of Microscopy*, **195**, 217–225.

RAMSAY, J. G. 1980. Shear zone geometry: a review. *Journal of Structural Geology*, **2**, 83–99.

REDDY, S. M., WHEELER, J. & CLIFF, R. A. 1999. The geometry and timing of orogenic extension: an example from the Western Italian Alps. *Journal of Metamorphic Geology*, **17**, 573–589.

REDDY, S. M., WHEELER, J. *et al.* 2003. Kinematic reworking and exhumation within the convergent Alpine Orogen. *Tectonophysics*, **365**, 77–102.

ROBIN, P. Y. F. & CRUDEN, A. R. 1994. Strain and vorticity patterns in ideally ductile transpression zones. *Journal of Structural Geology*, **16**, 447–466.

SANDERSON, D. J. & MARCHINI, W. R. D. 1984. Transpression. *Journal of Structural Geology*, **6**, 449–458.

TAKESHITA, T., TOMÉ, C., WENK, H.-R. & KOCKS, U. F. 1987. Single-crystal yield surface for trigonal lattices: Application to texture transitions in calcite polycrystals. *Journal of Geophysical Research*, **92**, 12917–12930.

TIKOFF, B. & TEYSSIER, C. 1994. Strain modeling of displacement-field partitioning in transpressional orogens. *Journal of Structural Geology*, **16**, 1575–1588.

TIKOFF, B. & GREENE, D. 1997. Stretching lineations in transpressional shear zones: an example from the Sierra Nevada Batholith, California. *Journal of Structural Geology*, **19**, 29–39.

TURNER, F. J. & HEARD, H. C. 1965. Deformation in calcite crystals at different srain rates. *University of California Publications in Geological Sciences*, **46**, 103–126.

WHEELER, J., REDDY, S. M. & CLIFF, R. A. 2001*a*. Kinematic linkage between internal zone extension and shortening in the more external units in the NW Alps. *Journal of the Geological Society, London*, **158**, 439–443.

WHEELER, J., PRIOR, D. J., JIANG, Z., SPEISS, R. & TRIMBY, P. W. 2001*b*. The petrological significance of misorientations between grains. *Contributions to Mineralogy and Petrology*, **141**, 109–124.